Building and Environment, Vol. 24, No. 1, pp. 73–84, 1989.
Printed in Great Britain.

0360–1323/89 $3.00+0.00

Application of Computational Fluid Dynamics in Room Ventilation

H. B. AWBI*

This paper presents the results of a computer program developed for solving 2- and 3-D ventilation problems. The program solves, in finite difference form, the steady-state conservation equations of mass, momentum and thermal energy. Presentation of the fluctuating velocity components is made using the k–ε turbulence model. Predicted results of air velocity and temperature distribution in a room are corroborated by experimental measurements. The numerical solution is extended to other room ventilation problems of practical interest.

NOMENCLATURE

A	area
Ar	Archimedes number ($\beta g h \Delta T_0 / U_0^2$)
a_i	coefficient of finite difference equation
C_1, C_2, C_D, C_μ	constants of turbulence equations
C_e	entrainment coefficient
C_p	specific heat
E	logarithmic law constant (9.793)
f	relaxation factor
G	large value
g	gravitational acceleration
H	room height
h	height of supply slot
I	inertia relaxation factor
k	kinetic energy of turbulence ($\frac{1}{2}u_i u_i$)
L	room length
Pe	local Peclet number ($\rho U \delta x / \Gamma$)
p	pressure
Q	volume flow rate
Re	Reynolds number ($U_0 h / \nu$)
S	Source term
T, T'	mean, fluctuating temperature
T^+	non-dimensional heat flux temperature
ΔT_0	difference between inlet and reference temperature ($T_o - T_r$)
t	time
U, V, W	mean velocity components in x, y, z direction
U_i, u_i	mean, fluctuating velocity component in x_i direction
u_τ	friction velocity ($\sqrt{\tau_w/\rho}$)
u^+	non-dimensional velocity (u/u_τ)
$\bar{V}$	mean resultant velocity in a horizontal plane
x, y, z	longitudinal, vertical and lateral coordinates
x_i	coordinate in tensor notation
y^+	local Reynolds number ($u_\tau y/\nu$)

Greek symbols

β	volumetric expansion coefficient
Γ	diffusion coefficient
γ	thermal conductivity
δ	Kronecker delta (0 if $i \neq j$ and 1 if $i = j$)
ε	turbulence energy dissipation rate
κ	Karman's constant (0.4187)
λ	turbulence constant
μ	laminar viscosity
μ_t	turbulent or eddy viscosity
ν	kinematic viscosity (μ/ρ)
ρ	fluid density
σ	Prandtl number ($\mu C_p/\gamma$)
σ_t	turbulent Prandtl (Schmidt) number
τ_w	wall shear stress
ϕ	dependent variable.

Subscripts

B	buoyancy
e	exit
i, j	vector directions
k	kinetic energy
m	maximum
o	inlet
p	grid or sink
r	room or reference
t	turbulent
u	source
ε	kinetic energy dissipation

Superscripts

′	old value
r	new value.

* Mechanical and Industrial Engineering Department, Napier Polytechnic, Colinton Road, Edinburgh, U.K.

1. INTRODUCTION

THE MEASURE of success of an air conditioning system design is normally assessed by the thermal conditions provided by the system in the occupied zones of a building. Although the thermal condition of the air supply may be finely tuned at the plant to offset the sensible and latent heat loads of the rooms, the thermal condition in the room is ultimately determined by the method of distributing the air into the room. Fanger and Pedersen [1] have shown that the thermal comfort in a room is not only affected by how uniform the air temperature and air velocity are in the occupied zone (the lower part of a room to a height 2 m) but also by the turbulence intensity of the air motion and the dominant frequency of the flow fluctuations. These environmental parameters which have profound influence on comfort, are influenced by the method used to diffuse the air into the room. In addition to the supply air velocity and temperature, the size and position of the diffuser in the room have a major influence on the thermal condition in the occupied zone [2].

In air distribution practice, ceilings and walls are very common surfaces which are used for diffusing the air jet so that when this penetrates the occupied zone its velocity would have decayed substantially. Thus the occurrence of draughts is minimized. The region between the ceiling and the occupied zone serves as an entrainment region for the jet which causes a decay of the main jet velocity as a result of the increase in the mass flow rate of the jet.

There are sufficient information and design guides [3, 4] which may be applied for predicting room conditions produced by conventional air distribution methods. However, where non-conventional methods of air supply are employed or where surface protrusions or rough surfaces are used in a wall-jet supply, the design data is scarce. The air distribution system designer has to rely on data obtained from a physical model of the proposed air distribution method. Modifications to these models are then made until the desired conditions are achieved. Apart from being costly and time consuming, physical models are not always possible to construct at full scale. Air distribution studies for the design of atria, theatres, indoor stadiums etc. can only be feasibly conducted with reduced scale models. However, tests carried out in a model should be made with dynamic and thermal similarity if they are to be directly applied to the full scale. This normally requires the equality of the Reynolds number, Re, and the Archimedes number, Ar, [5, 6] which is not possible to achieve in the model concurrently.

The other problem which is often encountered in air distribution design is the interference to the jet from rough surfaces and surface-mounted obstacles such as structural beams, light fittings etc. Previous studies [7, 8] have shown that surface-mounted obstacles cause a faster decay of the jet velocity and when the distance of an obstacle from the air supply is less than a certain value called "the critical distance", a deflection of the jet into the occupied zone takes place. This phenomenon renders the air distribution in the room ineffective in removing the heat load and, as a result, the thermal comfort in the occupied zone deteriorates. Here again there is a scarcity of design data, particularly for non-isothermal air jets.

Air distribution problems, such as those discussed here, are most suitable for numerical solutions which, by their nature, are good design optimization tools. Since most air distribution methods are unique to a particular building a rule of thumb approach is not often a good design practice. For this reason, a mock-up evaluation has so far been the safest design procedure. Therefore, numerical solutions are most suitable for air distribution system design as results can be readily obtained and modifications can be made as required within a short space of time. Because of the complexity of the air flow and heat transfer processes in a room, the numerical solutions to these flow problems use iterative procedures that require large computing time and memory. Therefore, rigorous validation of these solutions is needed before they can be applied to wide ranging air distribution problems.

In this paper a review is given of published work on numerical solutions as applied to room ventilation. The finite volume solution procedure which has been widely used in the past is briefly described and the equations used in the k–ε turbulence model are presented. Numerical solutions are given for two- and three-dimensional flows and, where possible, comparison is made with experimental data. The boundary conditions used in these solutions are also described.

2. PREVIOUS WORK ON NUMERICAL SOLUTIONS

Recently, there has been a lot of activity in developing general fluid flow and heat transfer programs for solving the flow of air in rooms. Most of the room flow programs currently in use are based on the work carried out at Imperial College by Patankar and Spalding [9, 10], Gosman [11] and their coworkers. Nielsen [12] developed a calculation procedure based on a stream function approach for predicting two-dimensional flow patterns in ventilated rooms. Later, Nielsen *et al.* [13, 14] used a finite volume solution of the 2-D equations for the conservation of mass, momentum and energy as well as the two equations for turbulence energy and its dissipation rate in the k–ε turbulence model. The solution procedure was then extended for solving a 3-D isothermal flow in ventilated rooms [15]. The effect of buoyancy was considered in [14] for a 2-D flow. For the cases considered the numerical predictions produced reasonable correlations with experimental data. Ideriah [16] used a similar numerical procedure to calculate the velocity and temperature fields in a ventilated 2-D square cavity with a heated ceiling. The predicted results showed a good comparison with experimental data. Markatos and Pericleous [17] obtained a solution to the natural convective flow in a square cavity with two differentially heated vertical walls and adiabatic horizontal floor and ceiling using the same equations and turbulence model as the previous investigators but applying a different procedure for solving these equations. A satisfactory correlation was obtained with published experimental data for both laminar and turbulent convection within the cavity. Markatos *et al.* [18] also solved the 2-D steady-state flow equations to predict the spread of fire in a room by representing the fire source by a heat source and adding additional terms to the equations for k and ε to prescribe the highly buoyant flows being simulated. This solution was later extended [19] to 3-D steady-state and transient flows including the effect of compressibility. Due to the limited experimental data available on the spread of fire, a partial validation of the numerical predictions was presented only for a steady-state flow.

Using the same numerical solution as Nielsen *et al.*, Reinartz and Renz [20] investigated the flow in a rectangular room ventilated by a ceiling plate diffuser for heating and cooling modes. The flow within the diffuser and in a vertical plane of the room containing the diffuser was well predicted by a 2-D solution. Kato and Murakami [21] used a 3-D solution for the velocity distribution and spread of contamination in downward flow clean rooms of different number of supply openings. In addition to the previously mentioned equations, a contaminant transport equation was also solved. The general flow pattern and the contaminant concentration was satisfactorily predicted for six different air supply configurations. Alamdari *et al.* [22] developed a similar computational procedure and used the k–ε turbulence model to predict the heat transfer coefficients for the internal

surfaces of a room heated by a 3-D warm air jet. The purpose of their work was to calculate the distribution of heat transfer coefficients over the room surfaces and to use this in thermal simulation programs. The average values for the walls, ceiling and floor were generally in agreement with the CIBSE recommended values.

Awbi and Setrak [23, 24] developed a numerical solution procedure based on the Imperial College work to predict the diffusion of an isothermal and non-isothermal plane wall jet. The effect of surface mounted rectangular obstacles of different dimensions on the diffusion of the wall jet was also studied and a good agreement with experimental data was obtained. The deflection of the jet and its separation from the surface was accurately predicted by the numerical solution. The influence of a wall opposite the air supply on the diffusion of the wall jet in the vicinity of the wall was also investigated. The effect of the wall on the jet was found to be more than had been previously expected. Whittle [25] used a similar program to predict the down draught near a cold window. A 2-D approximation was used to study the air flow in a room heated by a warm air jet supplied from a linear diffuser. The general flow pattern was reasonably predicted by the numerical solution.

At a recent conference in Stockholm [26] a total of six papers were presented on the prediction of air velocity and temperature distribution and the dispersion of contaminants in ventilated spaces using numerical solution procedures which are very similar to those described earlier. All these investigators used a finite volume solution of the flow equations and the equations for k and ε either in 2- or 3-D flow situations. For most cases where comparison with experimental results was made a reasonable correlation has been obtained.

3. NUMERICAL SOLUTION PROCEDURE

3.1. *Flow and energy equations*

The general equations describing the flow in a room can be represented as follows.

(i) Continuity equation:

$$\frac{\partial \rho}{\partial t} + \frac{\partial}{\partial x_i}(\rho U_i) = 0. \tag{1}$$

(ii) Momentum (Navier–Stokes) equation:

$$\frac{\partial}{\partial t}(\rho U_i) + \frac{\partial}{\partial x_j}(\rho U_i U_j) = -\frac{\partial p}{\partial x_i} + \frac{\partial}{\partial x_j}(-\rho\overline{u_i u_j}) + \frac{\partial}{\partial x_j}\left[\mu\left(\frac{\partial U_i}{\partial x_j} + \frac{\partial U_j}{\partial x_i}\right)\right] + g_i(\rho - \rho_r). \tag{2}$$

(ii) Thermal energy equation:

$$\frac{\partial}{\partial t}(\rho T) + \frac{\partial}{\partial x_j}(\rho U_j T) = \frac{\partial}{\partial x_i}(-\rho\overline{u_i T'}). \tag{3}$$

In these equations U_i represents the time-mean velocity component in the x_i direction and u_i is the fluctuating velocity components in the x_i direction. The other quantities are defined in the nomenclature. For turbulent flows, as in the flow of air in rooms, the viscous stress term on the right hand side of Equation (2) is usually much smaller than the Reynolds stress term preceding it in the equation and is therefore neglected. If a steady incompressible flow is assumed and the fluctuating velocities are described by a suitable turbulence model which represents the effect of a fluctuating flow by means of time-independent flow equations, then Equations (1)–(3) reduce to:

$$\frac{\partial}{\partial x_j}(\rho U_i) = 0 \tag{4}$$

$$\frac{\partial}{\partial x_j}(\rho U_i U_j) = -\frac{\partial p}{\partial x_i} + \frac{\partial}{\partial x_j}(-\rho\overline{u_i u_j}) + g_i(\rho - \rho_r) \tag{5}$$

$$\frac{\partial}{\partial x_j}(\rho U_j T) = \frac{\partial}{\partial x_i}(-\rho\overline{u_i T'}). \tag{6}$$

3.2. *Turbulence model*

To solve Equations (5) and (6) it is necessary to represent the fluctuating velocity term in Equation (5) and the fluctuating temperature term in Equation (6) by "equivalent" time-mean terms. For this purpose a model of turbulence is required. There are a number of models which can be used, e.g. see Rodi [27]. However, these models vary in complexity by the number of additional equations that need to be solved. All these models are semi-empirical and therefore do not normally produce the same results. One of the most widely used turbulence models is the two equation model of kinetic energy, k, and its dissipation rate, ε. This model, which is usually referred to as the k–ε model, has been applied by most investigators who studied the numerical solution of air flow in rooms and cavities [11–26] and it is also used for the present work. The Reynolds stresses in Equation (5) are represented by the product of the eddy viscosity, μ_t, and the mean velocity gradient thus:

$$-\rho\overline{u_i u_j} = \mu_t\left(\frac{\partial U_i}{\partial x_j} + \frac{\partial U_j}{\partial x_i}\right) - \frac{2}{3}\rho k\delta_{ij}, \tag{7}$$

where the turbulence kinetic energy k is given by:

$$k = \tfrac{1}{2}\overline{u_i u_i} \tag{8}$$

and δ_{ij} is the Kronecker delta $= \begin{Bmatrix} 100 \\ 010 \\ 001 \end{Bmatrix}$.

Substituting Equation (7) in (5) gives:

$$\frac{\partial}{\partial x_j}(\rho U_i U_j) = -\frac{\partial p}{\partial x_i} + \frac{\partial}{\partial x_j}\left[\mu_t\left(\frac{\partial U_i}{\partial x_j} + \frac{\partial U_j}{\partial x_i}\right) - \frac{2}{3}\rho k\delta_{ij}\right] + g_i(\rho - \rho_r). \tag{9}$$

Similarly the turbulent heat flux term in Equation (6) is represented by the product of a turbulent diffusion coefficient, Γ_t, and the mean temperature gradient, thus:

$$-\rho\overline{u_i T'} = \Gamma_t\frac{\partial T}{\partial x_i}, \tag{10}$$

where

$$\Gamma_t = \mu_t/\sigma_t. \tag{11}$$

The model relates the eddy viscosity to the local values

of ρ, k and ε by the expression:

$$\mu_t = C_\mu \rho k^2/\varepsilon, \tag{12}$$

where C_μ is an empirical value which is constant for high Reynolds number flows. Substituting Equation (10) in (6) gives:

$$\frac{\partial}{\partial x_j}(\rho U_j T) = \frac{\partial}{\partial x_i}\left(\Gamma_t \frac{\partial T}{\partial x_i}\right). \tag{13}$$

The transport equations of k and ε for a steady buoyant and high Reynolds number flow are:

$$\frac{\partial}{\partial x_i}(\rho U_i k) = \frac{\partial}{\partial x_i}\left(\Gamma_k \frac{\partial k}{\partial x_i}\right) + \rho(S_k + S_B) - C_D \rho \varepsilon, \tag{14}$$

$$\frac{\partial}{\partial x_i}(\rho U_i \varepsilon) = \frac{\partial}{\partial x_i}\left(\Gamma_\varepsilon \frac{\partial \varepsilon}{\partial x_i}\right) + C_1 \rho \frac{\varepsilon}{k}(S_k + S_B) - C_2 \rho \frac{\varepsilon^2}{k}. \tag{15}$$

The source terms for turbulent kinetic energy, S_k, and buoyancy, S_B, are presented by the following expressions:

$$S_k = \frac{\mu_t}{\rho}\frac{\partial U_i}{\partial x_j}\left(\frac{\partial U_i}{\partial x_j} + \frac{\partial U_j}{\partial x_i}\right), \tag{16}$$

$$S_B = -\beta g \frac{\mu_t}{\rho \sigma_t}\frac{\partial T}{\partial x_j}. \tag{17}$$

The diffusion coefficients Γ_k and Γ_ε are given by:

$$\Gamma_k = \mu_t/\sigma_k \tag{18}$$

and

$$\Gamma_\varepsilon = \mu_t/\sigma_\varepsilon. \tag{19}$$

The empirical constants in the turbulence model equations are assigned the values given in Table 1. Similar values have been used by other investigators [14, 16, 17, 20, 22] however, Nielsen *et al.* [14] used an expression for σ_t based on boundary layer measurements and Ideriah [16] also applied a similar expression for σ_t. The present investigation has shown that using such expressions does not improve the numerical solution for air flow in rooms and as a result σ_t was taken to have a constant value of 0.75. Other investigators have also assumed a constant value for σ_t between 0.5 and 0.9.

3.3. *Boundary conditions*

The equations described in the previous sections were solved to predict the air velocity and temperature distribution in: (i) mechanically ventilated (heated or cooled) rooms; (ii) wall jet flow over a surface-mounted obstacle. Since the boundary conditions are unique to a particular flow situation, an accurate representation of these conditions is necessary for a reliable solution to be achieved. For the ventilated rooms it is necessary to specify the conditions at inlet, outlet and on the internal surfaces of the room. In the case of the wall jet there is a free boundary parallel to the wall over which the jet diffuses, where entrainment of surrounding air occurs, as well as the boundaries of the obstacles attached to the wall. Therefore, in addition to the inlet, outlet and wall boundary conditions for a room, boundary conditions are required for the entrainment boundary and the obstacles. In general, five types of boundary conditions were used in the present solutions.

Table 1. Empirical constants in the turbulence model equations

C_μ	C_D	C_1	C_2	σ_k	σ_ε	σ_t
0.09	1.0	1.44	1.92	1.0	1.22	0.75

3.3.1. *Inlet conditions.* Uniform distribution is used over the inlet boundary of the longitudinal velocity, U_0, temperature, T_0, kinetic energy of turbulence, k_0, and the energy dissipation rate, ε_0. Where comparison is made with experimental results, the inlet conditions are obtained from the measured quantities at inlet. Where experimental data are not available, assumed values are used which are considered to represent the problem in hand. Other quantities such as pressure and the other two velocity components are taken as zero at the inlet. The kinetic energy of turbulence is calculated using:

$$k_0 = \tfrac{3}{2} I_u^2 U_0^2, \tag{20}$$

where I_u^2 is the turbulence intensity of the u-component of velocity at the inlet which is taken as 0.14 in the absence of measured values. The dissipation rate is obtained from:

$$\varepsilon_0 = k_0^{1.5}/(\lambda H), \tag{21}$$

where λ is a constant taken as 0.005 and H is the room height or the square root of the cross-sectional area of the room. Calculations with different values of k_0 and ε_0 showed little effect on the results.

3.3.2. *Exit conditions.* The longitudinal component, U_e, is derived from the continuity equation, i.e.

$$U_e = U_0 \frac{A_0}{A_e}\frac{\rho_0}{\rho_e},$$

and the other velocity components and the pressure are assumed to be zero. The exit temperature T_e is obtained from the energy equation for the whole flow field taking into account heat transfer across all boundaries. Boundary conditions for k and ε are not required because an up-wind computational scheme, described later, is used except that their gradients in the exit plane are zero. Uniform distribution of U_e and T_e is also assumed across the exit area.

3.3.3. *Wall boundary.* Close to a wall region laminar viscosity becomes more significant than turbulent viscosity as a result of the damping effect of the wall, i.e. $(\partial k/\partial y)_{wall} = 0$. Therefore, the turbulence model Equations (14) and (15) do not apply to regions close to a solid boundary and instead the wall-function equations due to Launder and Spalding [28] are used for the velocity component parallel to the boundary. Within the laminar sublayer region, i.e. $y^+ \leqslant 11.63$ viscous effects predominate and the wall shear stress, τ_w, is described by the usual Couette flow expression, i.e. $u^+ = y^+$ and $T^+ = \sigma y^+$. At a point outside this region turbulent shear becomes significant and it can be shown that when the generation and dissipation of energy is in balance then $\tau/\rho = C_\mu^{1/2} k$ and the following expressions for momen-

tum and heat fluxes are used for $y^+ > 11.63$:

$$u^+ = \frac{1}{\kappa}\ln(Ey^+), \tag{22}$$

$$T^+ = \frac{\rho u_\tau C_p(T_w - T)}{q_w} = \sigma_t\left[u^+ + f\left(\frac{\sigma}{\sigma_t}\right)\right], \tag{23}$$

where $f(\sigma/\sigma_t)$ is a function of the ratio σ/σ_t given in reference [16] as:

$$f\left(\frac{\sigma}{\sigma_t}\right) = 9.24\left[\left(\frac{\sigma}{\sigma_t}\right)^{0.75} - 1\right] \times\left\{1 + 0.28\exp\left[-0.007\left(\frac{\sigma}{\sigma_t}\right)\right]\right\}.$$

The boundary temperatures can be specified to represent the actual temperatures of the room surfaces or to represent the temperature of a heat source or sink of a known capacity. Heat fluxes or sinks can be treated as additional source terms in the energy equation.

3.3.4. *Obstacle boundary.* The source terms in the finite difference equation (see section 3.4) are expressed as "false" source terms in the obstacle domain so that in Equation (26):

$$S_u = G\phi_p,$$

and

$$S_p = -G,$$

where G is a large value, e.g. 10^{30}. At the obstacle boundaries the momentum and heat fluxes are expressed by the wall functions for a solid boundary, i.e. Equations (22) and (23).

3.3.5. *Free entrainment boundary.* A wall jet entrains fluid at its free boundary (shear layer boundary) and when solving for this type of problem entrainment conditions are specified at the free boundary of the flow field. The conditions are such that the longitudinal velocity component is zero and the vertical entrainment velocity given by:

$$U_j = C_e U_m, \tag{24}$$

is imposed at the boundary. In this equation U_m is the maximum longitudinal velocity in a vertical plane across the jet and C_e is an entrainment coefficient. For a plane wall jet (2-D jet) $C_e = 0.035$ [29] and for a 3-D wall jet C_e may be taken as 0.03 [30]. The temperature at the boundary is the bulk temperature of the fluid surrounding the jet.

3.4. *Finite volume solution*

Equations (4), (9) and (13)–(15) all have the general form:

$$\frac{\partial}{\partial x_i}(\rho U_i\phi) = \frac{\partial}{\partial x_i}\left(\Gamma_\phi\frac{\partial\phi}{\partial x_i}\right) + S_\phi, \tag{25}$$

where S_ϕ represents source terms of the dependent variable ϕ. The expression for S_ϕ in the continuity, momentum, thermal energy, turbulence energy and energy dissipation equations can be easily deduced by comparing Equation (25) with the corresponding equations given earlier. In the momentum equation Γ_ϕ is represented by the turbulence viscosity μ_t.

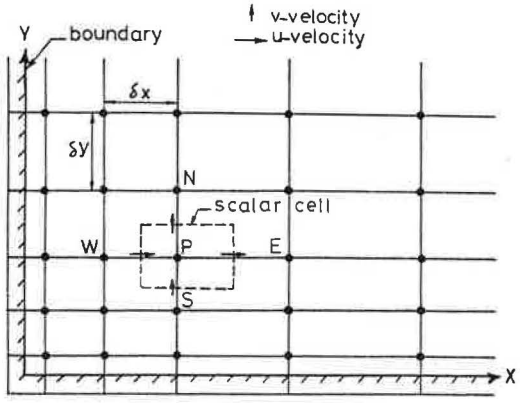

Fig. 1. Two-dimensional grid and control volume.

Using a rectangular finite difference grid for the flow domain (Fig. 1), Equation (25) may be discretised by integration (summation) over an element control volume or cell to yield an algebraic equation of the form:

$$(\Sigma a_i - S_p)\phi_p = \Sigma(a_i\phi_i) + S_u, \tag{26}$$

which relates nodal values of the variable at node P, ϕ_p, to values at six neighbouring nodes, ϕ_i, for a 3-D flow field (N, S, E, W, L, R) or four neighbouring nodes for a 2-D flow (N, S, E, W). The coefficient a_i in the finite difference equation (Equation (26)) links the convective and diffusive terms of the differential equation between cell P and cell i. S_u and S_p are the source and sink terms of cell P and the term $(S_u + S_p\phi_p)$ is integrated over the cell. This method of solution is referred to as the SIMPLE algorithm which is described by Patankar [10] and has been used extensively for solving elliptic flow problems. This method does not employ equations for pressure, instead the pressure in each computational cell is linked to the velocities of the surrounding cells in such a way that conformity with the continuity equation is always observed. This yields a pressure correction equation which gives the pressure change needed to obtain the necessary change in the velocity and/or density so that continuity of flow is satisfied. This procedure is described in detail by Markatos *et al.* [18]. For this reason it is necessary to use a staggered grid as shown in Fig. 1, where the scalar quantities (p, T, k, ε) are located at point P (grid nodes) and the velocity components U, V and W are located at the boundaries of the scalar cell. The grid is arranged in such a way that boundaries coincide with control volume walls. At a solid boundary a wall function is used for the points close to the wall. Depending on the Reynolds number of the cell this can either be an expression for laminar or turbulent boundary layers.

The finite difference scheme used for solving Equation (25) is hybrid depending on the value of the Peclet number ($Pe = \rho U\delta x/\Gamma$) for the cell. A central differencing is used for $|Pe| < 2$ and an up-wind differencing (taking a value of Φ_i for the up-wind node) is used for $|Pe| \geqslant 2$. This scheme is used to enhance computational stability.

The discretized equations are solved by sweeping the flow field plane-by-plane for a 3-D flow or line-by-line for 2-D field at a given x-position starting from top to bottom. The tri-diagonal matrix algorithm (TDMA) is applied for solving the discretized equations. The pro-

cedure is repeated for the next plane or line downstream until the whole field is swept.

3.5. *Computer program*

A 2-D program is used to simulate the heating and cooling of two rooms using slot diffusers across the full width of each room. A 3-D program which is an extension of the 2-D one is used to simulate the flow of a wall jet over an obstacle. Both versions were initially validated using published data on the diffusion of 2- and 3-D wall jets. For the 2-D program a non-uniform grid is used in the x- and y-directions to produce a very fine grid near the internal surfaces and a coarse grid in the central region of the room. The size of the grid in the x- and y-directions is 42×38 respectively. For the 3-D program non-uniform grids are used in the x- and y-directions and a uniform grid in the z-direction ($20 \times 20 \times 11$). Very fine grids are used close to the inlet of the jet and near the obstacles and these become coarser with distance from the inlet and from the obstacle.

For solving non-isothermal flows, numerical stability is enhanced by choosing the correct relaxation factors f. With reference to Equation (26), f is defined as:

$$\phi_p^r = f\phi_p + (1-f)\phi_p', \tag{27}$$

where ϕ_p' is the value of ϕ_p from the previous sweep, ϕ_p is the value calculated from Equation (26) and ϕ_p^r is the new value using the relaxation factor. A value of $f = 0.5$ is used for the velocity components, k and ε and a value of 1.0 for p and T.

When non-isothermal flow solutions are performed, the above stability measure was found sometimes to produce unconverged solutions. As a result the inertia relaxation method of Ideriah [16] was used for solving the vertical velocity component, V, in which case stable solutions were achieved for most cases considered. Using this method, Equation (26) for the V-component is written in the following form:

$$\phi_p = \frac{\Sigma(a_i\phi_i) + S_u + I\phi_p'}{\Sigma a_i - S_p + I} \tag{28}$$

where I is an inertia relaxation factor defined by:

$$I = \frac{\alpha\rho g\beta(T_p - T_r)}{\sqrt{g\beta T_r L}}.$$

A value of 0.2 is used for α and L is the length of flow field in the x-direction. In Equation (28) the absolute value of I is used.

Applying this solution procedure a converged solution is usually achieved after about 500 iterations. The boundary conditions are imposed for each iteration during which the field is swept three times for each variable except p for which five sweeps are used. Convergence was reached when the sum of the mass flow residues for all node points was less than the mass flow rate. For a 2-D problem a CPU time of about 35 min is required using a Prime 9955. This extends to about 100 min for a 3-D problem.

4. RESULTS AND DISCUSSION

4.1. *Velocity and temperature distribution*

Using the 2-D program the velocity and temperature distribution were predicted for a test room which was designed for evaluating the performance of ceiling diffusers [31]. The room has a square floor of length 4.2 and height 2.8 m. In this instant, the air is supplied from a 24 mm continuous slot diffuser (type AK25/2) in the ceiling spanning the width of the room and at a distance 1.2 m from the wall. The room load was produced by electrically heated tapes laid over the floor area to produce a uniform load distribution. For these reasons a 2-D solution was used to predict the air movement in the test room.

Figure 2 shows the velocity distribution in the occupied zone of the room for different air flow rates and supply temperature. The air velocities were measured with TSI

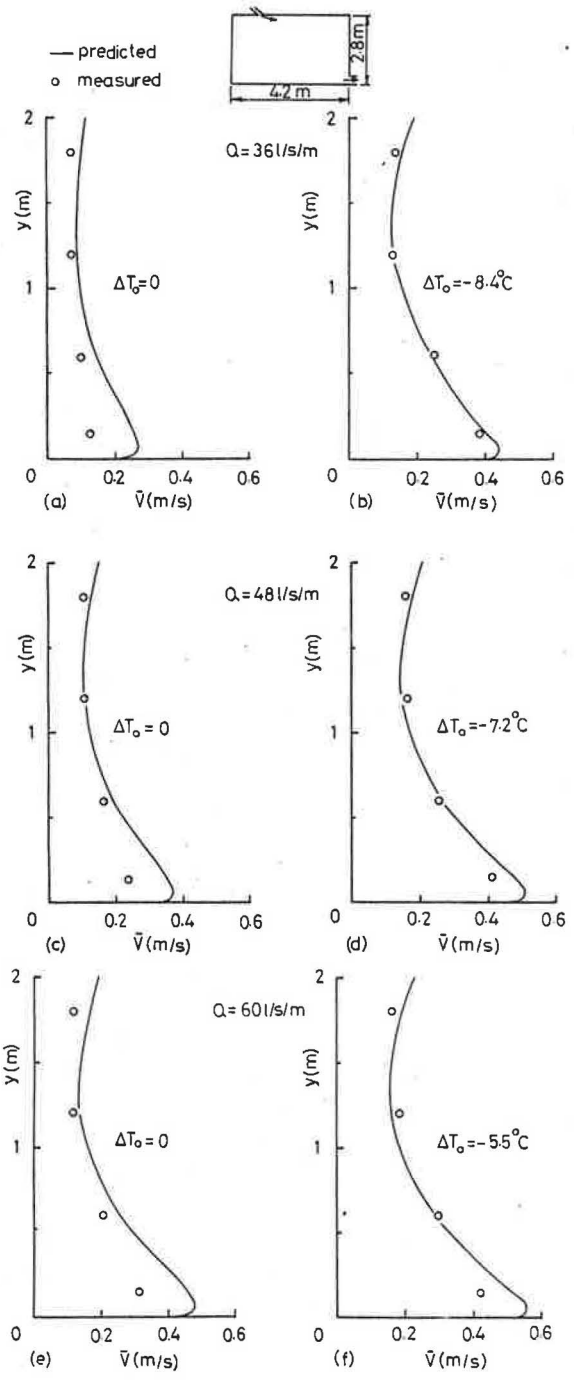

Fig. 2. Mean velocity profiles in the occupied zone.

1610 low velocity anemometers which give the magnitude of velocity at the measuring point. The velocities shown in Fig. 2 represent the magnitude of the mean velocities in horizontal planes of the occupied zone. For this purpose the occupied zone has been defined as the region extending from the floor to a height of 2 m above the floor and up to a distance of 0.15 m from the walls. However, the measurements were carried out using square grids of 1 and 0.5 m at distances of 0.15, 0.6, 1.2 and 1.8 m above the floor. The predicted velocity profiles are close to the experimental profiles except near the floor where the predicted values are higher particularly for the isothermal tests. The average velocity at a height of 0.15 m for the test with the lowest flow rate (Fig. 2a) appears to be low in comparison with the corresponding values for the other isothermal tests (Figs 2c and e). At this height $\bar{V}/U_0$ for this test is 0.056 as compared to 0.075 and 0.079 for the other two tests. This could be attributed to the limitation of the low velocity anemometer in measuring velocities below 0.1 m s^{-1}. The results in Fig. 2 show a significant increase in the air velocities in the occupied zone when cold air is supplied to the room at high level.

The temperature profiles for the three non-isothermal tests of Fig. 2 are shown in Fig. 3. It can be seen that a uniform temperature distribution is produced and the predicted temperatures are within 0.5°C of the measured values. Since floor heating was used as the room load, the predicted temperatures show a steep gradient over a distance of 0.15 m from the floor. This region represents the thermal boundary layer which was beyond the range of experimental measurements. It should be noted that the thermocouples were provided with a radiation shield to reduce the effect of radiant temperature and this is clearly demonstrated by the values of measured temperatures near the floor which are close to the air temperatures predicted by the numerical solution.

The flow of air in the room is demonstrated by the velocity vector plots of Fig. 4 (a and b). In this figure the same flow rate is used but in Fig. 4b the supply

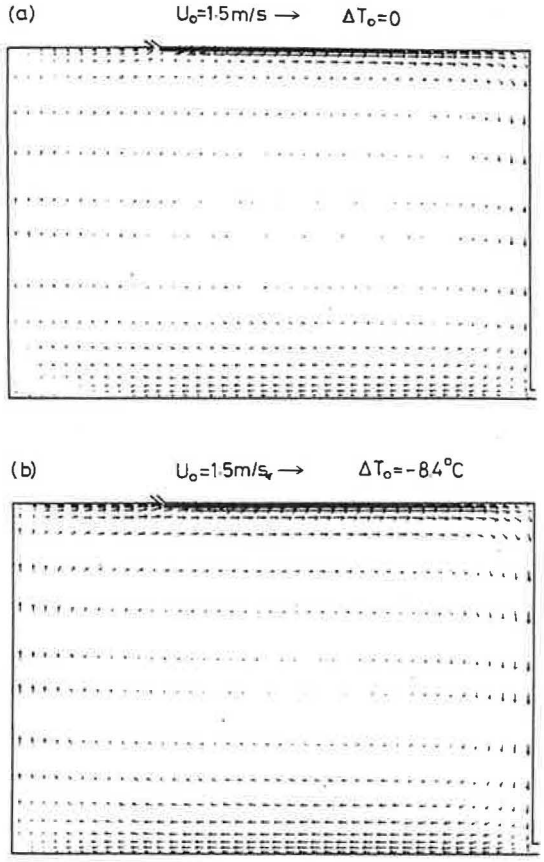

Fig. 4. Predicted velocity vectors in test room.

temperature differential, ΔT_0, is −8.4°C. The effect of buoyancy on the flow is to increase the velocity in the occupied zone and in particular close to the floor at about ankle level. A mean air velocity greater than 0.25 m s^{-1} is not expected to be tolerated by most people [32]. Therefore, the increase in air velocity with room load must be carefully considered when an air distribution

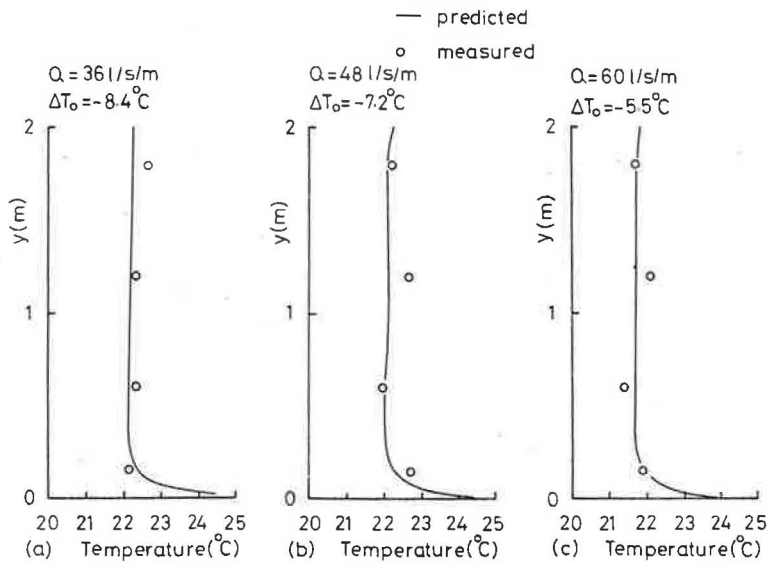

Fig. 3. Temperature profiles in the occupied zone.

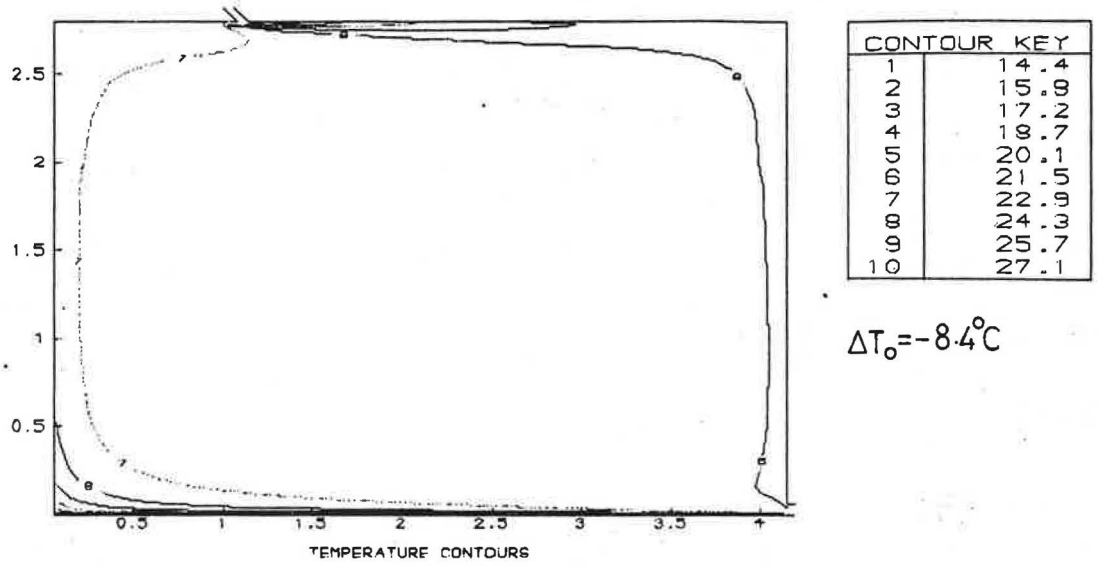

Fig. 5. Predicted temperature contours in test room.

system is designed. This is discussed further in the next section. Figure 5 shows a typical contour-plot of the predicted temperatures indicating the uniformity of temperature distribution in the occupied zone.

4.2. *Effect of Archimedes number*

The experimental measurements of Jackman [33] with central ceiling diffusers and slot ceiling diffusers positioned at the centre of the room and at one end of the room have shown that the average room air velocity depends on the type of air diffuser and its position, the momentum of the supply air and the room load. The room load affects the convective currents which are driven by the buoyancy force. The effect of buoyancy is normally represented by the value of Archimedes number, *Ar*, which is defined for the supply diffuser or the room. In the present work the diffuser parameters are used to define *Ar*. The effect of *Ar* on the mean velocity V_r in the occupied zone of the test room described earlier is shown in Fig. 6. These results have been obtained for a range of diffuser Reynolds numbers between 2400 and 4000. To isolate the effect of supply velocity change, the room velocity is plotted as a non-dimensional ratio of the supply velocity. In Fig. 6 the numerical predictions are in close agreement with experimental data and the results clearly demonstrate the significant influence of *Ar* on the room velocity. These cooling results show about 50% increase in room velocity for an increase of *Ar* from 4×10^{-4} to 4×10^{-3}.

The effect of cooling and heating on the mean room velocity is shown in Fig. 7 for a room with length 8.4 and height 2.8 m. The air is supplied along the ceiling from one end of the room where the wall is heated or cooled to simulate the room load. The results in Fig. 7 are predicted by a 2-D solution. In the cooling mode, the increase in room velocity with *Ar* is similar to the previous observations of Fig. 6. However, there is a substantial decrease in room velocity in the heating mode.

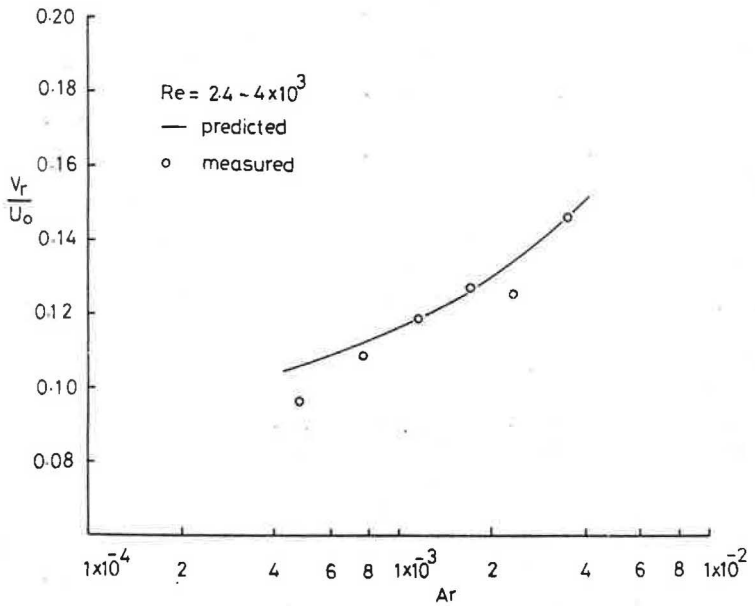

Fig. 6. Effect of Archimedes number on the mean velocity in the occupied zone.

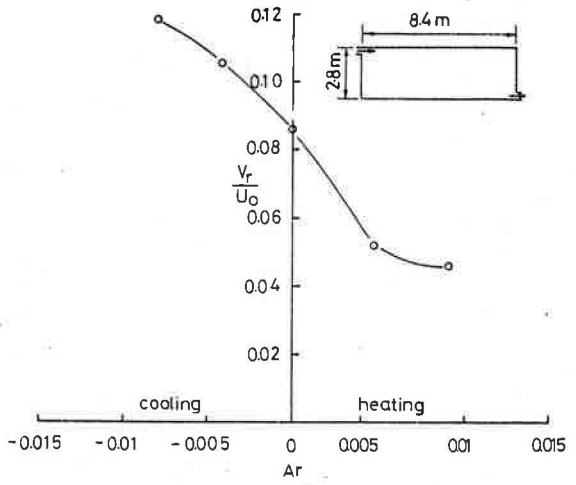

Fig. 7. Effect of heating and cooling on the mean velocity in the occupied zone.

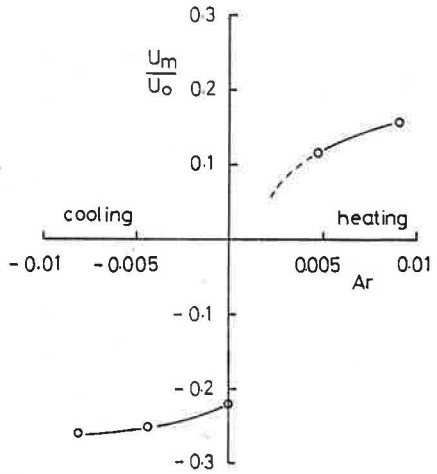

Fig. 8. Effect of Archimedes number on the maximum velocity near the floor.

Figure 8 shows the effect of cooling and heating on the maximum velocity near the floor of the 8.4 × 2.8 m room. For the isothermal and cooling modes the maximum velocity is negative and occurs close to the floor. As the temperature of the wall at the plane of the air supply opening decreases below the room temperature a downdraught is produced which counteracts the reverse flow close to the floor. Initially this causes a reduction in the reverse flow velocity but a situation is reached when the flow close to the floor will be produced by the downdraught which has a positive direction. In this case the flow is split into two regions dominated by two vortices of opposite circulation as shown in Fig. 9c. This type of air movement is highly undesirable because of the poor mixing of the supply air with room air and the resulting steep temperature gradients in the room. A similar situation could occur in the cooling mode (not shown by Fig. 9a) where the momentum of the supply jet is too low to counteract the downward buoyancy force acting on it causing it to "drop" into the occupied zone and producing two circulating zones at either end of the room.

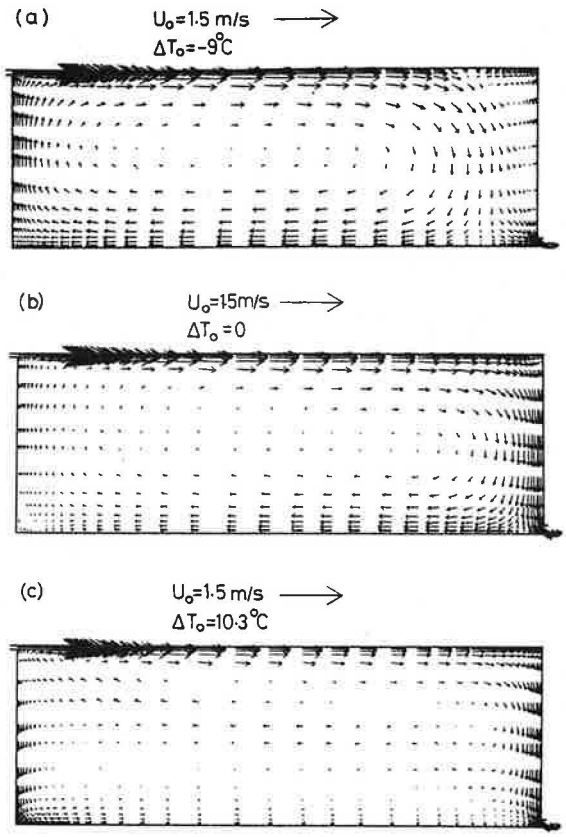

Fig. 9. Predicted velocity vectors for cooling, isothermal and heating modes.

4.3. *Effect of load*

Figure 10 shows the effect of the cooling load on the mean velocity in the occupied zone of the test room described earlier. For isothermal flows (zero loads) the mean velocity is strongly influenced by the momentum of the supply jet, hence the wide velocity band. However, as the cooling load increases the velocity band narrows

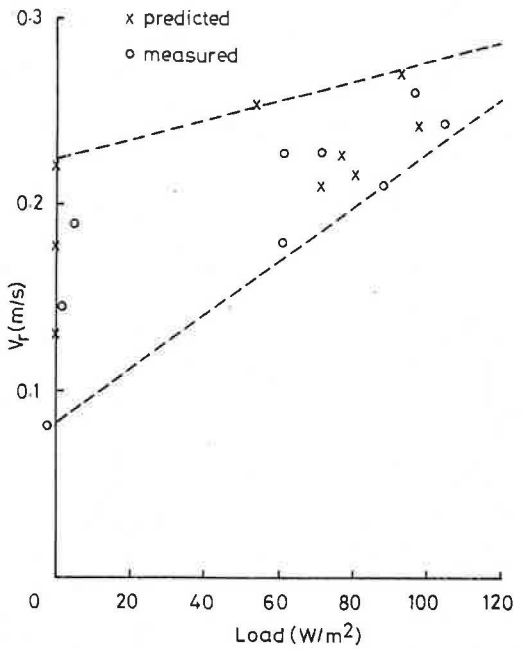

Fig. 10. Effect of load on mean velocity in the occupied zone.

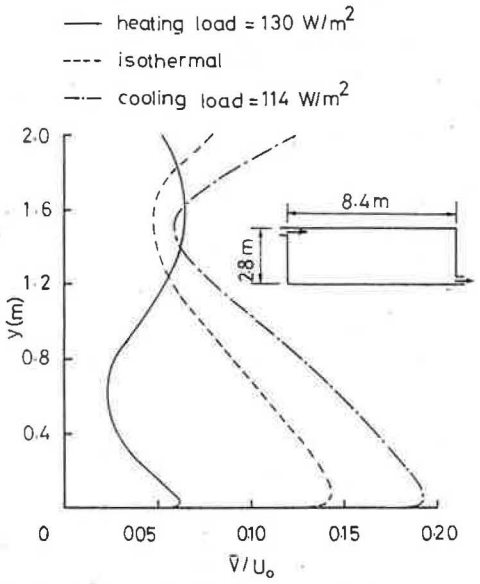

Fig. 11. Effect of room load in the mean velocity distribution in the occupied zone.

and for a load of 100 W m^{-2} the influence of the jet momentum becomes less significant and the velocity in the occupied zone is then influenced by the convective currents created by the buoyancy forces in the room. This figure also shows that the effect of room load on the velocity is more significant with low momentum air jets.

The predicted effect of heating and cooling loads on the mean velocity profile in the 8.4×2.8 room is shown in Fig. 11. The velocity in the lower region of the occupied zone increases when a cooling load is applied and decreases significantly when a similar value heating load is imposed. This is due to the opposite effect of buoyancy in heating and cooling. The gradients of the average temperature in the occupied zone are shown in Fig. 12 for heating and cooling for the same load values as Fig. 11. Although the jet momentum in both cases is identical, the down-draught from the cold wall with heating causes a steep temperature gradient in the occupied zone.

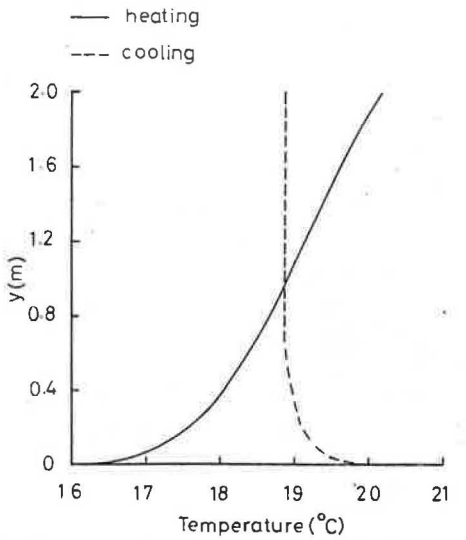

Fig. 12. Temperature profiles for heating and cooling.

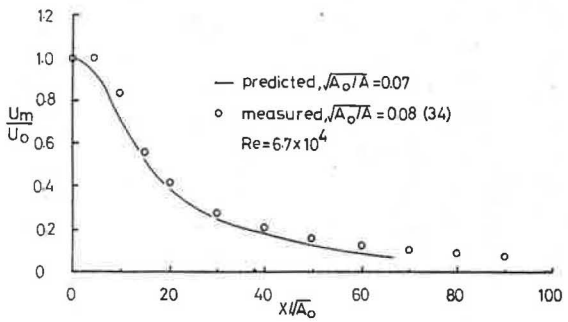

Fig. 13. Decay of maximum velocity for a 3-D wall jet.

4.4. *Effect of ceiling-mounted obstacles*

A study of the effect of a ceiling-mounted rectangular obstacle on the diffusion of a plane wall jet has been previously reported by the author and the results are published in references [23] and [24]. It was found that when the obstacle is placed at a distance from the supply slot below a critical value, x_c, the jet separates from the surface and if the obstacle distance $> x_c$ the jet reattaches to the surface downstream of the obstacle forming a recirculation "bubble". In both cases the diffusion of the jet is enhanced by the presence of the obstacle. Since these studies, the diffusion of a 3-D wall jet with and without an obstacle has been investigated and some predicted results are presented in Figs 13–15.

As a validation of the 3-D program which has evolved from the 2-D version, predicted results for a 3-D wall jet produced by a square opening were compared with experimental data given by Rajaratnam and Pani [34]. Figure 13 shows a comparison between the predicted

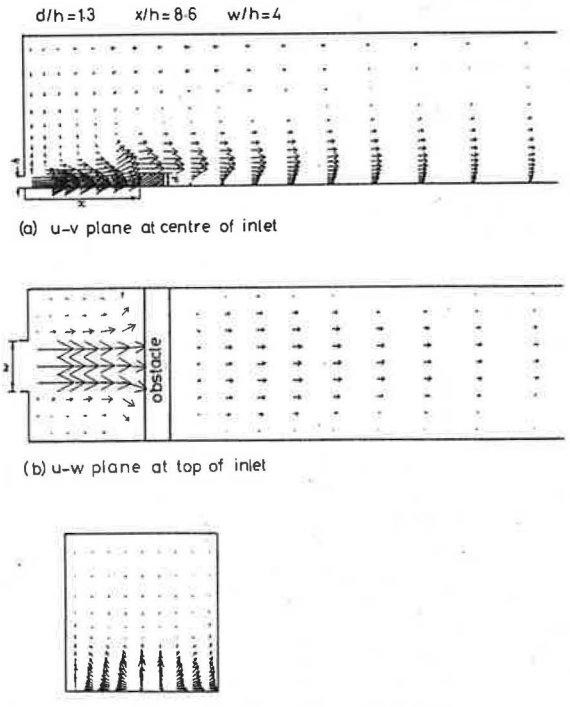

Fig. 14. Velocity vectors of the flow over an obstacle with reattached jet.

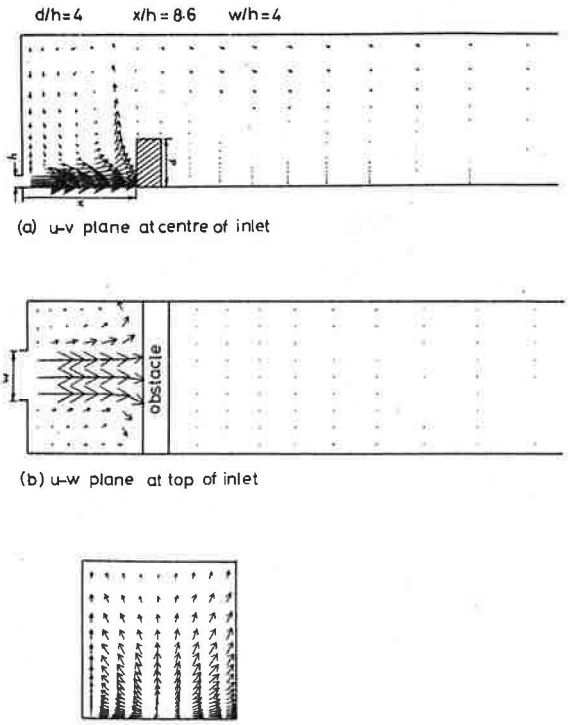

(a) u–v plane at centre of inlet

(b) u–w plane at top of inlet

(c) v–w plane at the grid section upstream of obstacle

Fig. 15. Velocity vectors of the flow over an obstacle with separated jet.

decay of the maximum velocity in the jet and the experimental results of reference [34] for values of $\sqrt{A_0 A}$ of 0.07 and 0.08 respectively where A is the cross-sectional area of the channel. It can be seen that the predicted velocities are in good agreement with the measured values for a long distance from the inlet opening. Figures 14 and 15 illustrate the flow of a 3-D wall jet over an obstacle using velocity vectors. In Fig. 14 the jet passes over the obstacle and reattaches back to the surface forming a recirculation bubble. When the height of the obstacle is increased, as in Fig. 15, the jet separates from the surface completely forming two recirculation zones.

5. CONCLUSIONS

A computational fluid dynamics (CFD) method has been described and applied to predict the air flow and heat transfer in 2-D enclosures and the 3-D flow of a wall jet over surface-mounted obstacles. The CFD solution produced reasonably good predictions of the air velocity and temperature distribution in a test room cooled by a ceiling jet. Other predictions involving the heating and cooling of a room and the flow of a wall jet over an obstacle, for which no experimental data were available, appear to be physically plausible. The role of CFD solutions in room ventilation designs has been shown to provide an enhancement of the design process. A CFD solution produces considerably more qualitative and quantitative information than is possible with physical model tests since measurements in low velocity turbulent flows do not usually provide a full description of the flow.

It must be mentioned, however, that considerably more work is necessary to validate the CFD programs in different room ventilation studies before they can be confidently used as design tools. In particular, other turbulence models should be investigated, e.g. the Reynolds stress model, as the accuracy of the k–ε model in predicting highly buoyant and low Reynolds number flows, such as naturally convected flows, has been found to be rather poor by some investigators. For such flows, the validity of the wall function expressions which were developed from measurements in turbulent boundary layers, is rather sceptical. The development of more realistic wall functions for buoyancy-dominated flows which can be easily incorporated in CFD programs will undoubtedly improve their prediction accuracy near solid boundaries.

Acknowledgement—The author is grateful to Martingale Technical Services Ltd. for supplying the experimental data used for validating some of the numerical predictions.

REFERENCES

1. P. O. Fanger and C. J. K. Pedersen, Discomfort due to air velocities in spaces. Proceedings of the Meeting of Commission E1 of the International Institute of Refrigeration, pp. 307–313, Belgrade (1977).
2. H. B. Awbi, Domestic warm air distribution with low-grade heat systems. Proceedings of the International Seminar on Energy Saving in Buildings (Edited by H. Ehringer and U. Zito), pp. 628–638, The Hague (1983).
3. P. J. Jackman, Air movement in rooms with side-wall mounted grilles: a design procedure. BSRIA Laboratory Report No. 65 (1970).
4. P. J. Jackman, Air movement in rooms with sill-mounted grilles: a design procedure. BSRIA Laboratory Report No. 71 (1971).
5. M. Rolloos, Possibilities and limitations for the prediction of air flow patterns, temperatures and velocities in large halls using scale models. Proceedings of the Meeting of Commission E1 of the International Institute of Refrigeration, pp. 245–256, Belgrade (1977).
6. W. Moog and F. Sodec, Raumströmungsuntersuchungen für das projekt Stadhalle Aachen. *Heiz.-Lüft-Haustech.* **27**, 390–400; 442–448 (1976).
7. M. J. Holmes and E. Sachariewicz, The effect of ceiling beams and light fittings on ventilation jets. BSRIA Laboratory Report No. 79 (1973).
8. P. V. Nielsen, The influence of ceiling-mounted obstacles on the air flow pattern in air-conditioned rooms at different heat loads. *Bldg Serv. Engng Res. Tech.* **1**, 199–203 (1980).
9. S. V. Patankar and D. B. Spalding, *Heat and Mass Transfer in Boundary Layers*. 2nd Edition. Intertext, London (1970).
10. S. V. Patankar, *Numerical Heat Transfer and Fluid Flow*. McGraw-Hill, New York (1980).

11. A. D. Gosman, E. E. Khalil and J. H. Whitelaw, The calculation of two-dimensional turbulent recirculating flows. Proceedings of the Symposium on Turbulent Shear Flows, Pennsylvania University (1977).
12. P. V. Nielsen, Flow in air conditioned rooms. Ph.D. Thesis, Technical University of Denmark (1974).
13. P. V. Nielsen, A. Restivo and J. H. Whitelaw, The velocity characteristics of ventilated rooms. *J. Fluids Engng* **100**, 291–298 (1978).
14. P. V. Nielsen, A. Restivo and J. H. Whitelaw, Buoyancy-affected flows in ventilated rooms. *Numerical Heat Transfer* **2**, 115–127 (1979).
15. A. D. Gosman, P. V. Nielsen, A. Restivo and J. H. Whitelaw, The flow properties of rooms with small ventilation openings. *J. Fluids Engng* **102**, 316–323 (1980).
16. F. J. K. Ideriah, Prediction of turbulent cavity flow driven by buoyancy and shear. *J. Mech. Engng Sci.* **22**, 287–295 (1980).
17. N. C. Markatos and K. A. Pericleous, Laminar and turbulent natural convection in an enclosed cavity. *Int. J. Heat Mass Transfer* **27**, 755–772 (1984).
18. N. C. Markatos, M. R. Malin and G. Cox, Mathematical modelling of buoyancy-induced smoke flow in enclosures. *Int. J. Heat Mass Transfer* **25**, 63–75 (1982).
19. N. C. Markatos and G. Cox, Hydrodynamics and heat transfer in enclosures containing a fire source. *PhysicoChemical Hydrodynamics* **5**, 53–66 (1984).
20. A. Reinartz and U. Renz, Calculations of the temperature and flow field in room ventilated by a radial air distributor. *Int. J. Refrig.* **7**, 308–312 (1984).
21. S. Kato and S. Murakami, Three-dimensional numerical simulation of turbulent air flow in ventilated room by means of 2-equation model. International Symposium Computation Fluid Dynamics, pp. 560–571, Tokyo (1985).
22. F. Alamadari, G. P. Hammond and W. S. Mohammad, Computation of air flow and convective heat transfer within space-conditioned rectangular enclosures. Proceedings of the 5th International Symposium on the Use of Computers for Environmental Engineering Related to Buildings, pp. 191–205, Bath (1986).
23. H. B. Awbi and A. A. Setrak, Numerical solution of ventilation air jet. Proceedings of the 5th International Symposium on the Use of Computers for Environmental Engineering Related to Buildings, pp. 236–246, Bath (1986).
24. H. B. Awbi and A. A. Setrak, Air jet interference due to ceiling-mounted obstacles. Proceedings of the International Conference on Air Distribution in Ventilated Spaces, Stockholm (1987).
25. G. E. Whittle, Numerical air flow modelling. BSRIA TN 2 (1987).
26. Session 3, Proceedings of the International Conference on Air Distribution in Ventilated Spaces, Stockholm (1987).
27. W. Rodi, Turbulence models and their application in hydraulics, International Association of Hydraulic Research (1979).
28. B. E. Launder and D. B. Spalding, The numerical computation of turbulent flows. *Comput. Methods Appl. Mech. Engng* **3**, 269–289 (1974).
29. N. Rajaratnam, *Turbulent Jets*. Elsevier, Amsterdam (1976).
30. A. A. Setrak, The effect of rectangular obstacles on the diffusion of a wall jet. Ph.D. Thesis, Napier Polytechnic, Edinburgh (1988).
31. S. J. Savin and K. Sayers, Private communications. Martingale Technical Services Ltd., Penn, Buckinghamshire, England (1986).
32. International Standard ISO 5219, Air distribution and air diffusion—Laboratory aerodynamics testing and rating of air terminal devices (1984).
33. P. J. Jackman, Air movement in rooms with ceiling-mounted diffusers. BSRIA Laboratory Report No. 81 (1973).
34. N. Rajaratnam and B. S. Pani, Three-dimensional wall jets, *Trans. Am. Soc. Civ. Engrs J. Hydraulics Div.* **100**, 69—83 (1974).